Exploring the Synergistic Interplay of Optical, Morphological, and Catalytic Features in Ga-doped ZnO Nanoparticles: Harnessing their Potential for Photocatalytic Dye Degradation under UV-Green Light Irradiation

Alessandra Piras,[a,b] *Chiara Olla,*[c] *Luca Fusaro,*[a] *Nikolay Tumanov,*[a] *An-Sofie Kelchtermans,*[b,d] *Dries De Sloovere,*[b,d,e] *Ken Elen,*[b,d,e] *Carlo Maria Carbonaro,*[c] *An Hardy,*[b,d,e] *Peter Adriaensens,*[f] *Carmela Aprile,*[a,*] *Marlies Van Bael*[b,d,e]

[a]University of Namur, Unit of Nanomaterials Chemistry, Department of Chemistry, NISM, Rue de Bruxelles, 61-5000 Namur, Belgium

[b]Hasselt University, DESINe Group, Institute for Materials Research (imo-imomec), Agoralaan Building D, 3590 Diepenbeek, Belgium

[c]University of Cagliari, Department of Physics, Cittadella Universitaria, I-09042 Monserrato, Italy

[d]EnergyVille, Thor Park 8320, 3600 Genk, Belgium

[e]Imec, Division Imomec, Wetenschapspark 1, 3590 Diepenbeek, Belgium

[f]Hasselt University, Analytical and Circular Chemistry (ACC), Institute for Materials Research (imo-imomec), Agoralaan Building D, 3590 Diepenbeek, Belgium

KEYWORDS: Nanomaterials, Ga-doped ZnO, γ-Ga_2O_3, ^{71}Ga-NMR, Rhodamine B, Photoluminescence, Heterogeneous Photocatalysis, Greenlight.

ABSTRACT

This work explores the synthesis and characterization of undoped ZnO, Ga-doped ZnO (Ga:ZnO), and γ-Ga_2O_3 quasi-spherical nanoparticles and their catalytic activity in Rhodamine B photodegradation under UV-visible light exposure. Gallium dopant incorporation into Ga:ZnO was confirmed by ICP-OES, FT-IR and powder XRD, maintaining the hexagonal wurtzite structure with an additional zinc gallium carbonate Layered Double Hydroxide (LDH) phase at higher dopant concentrations. TEM images revealed no significant alteration in the morphology or size of the nanoparticles. ^{71}Ga-NMR indicated the location of the gallium atoms within the ZnO lattice, showing coordination changes with increasing dopant concentration. Ga-doped ZnO nanoparticles demonstrated reduced efficiency under UV light compared to commercial references. γ-Ga_2O_3 exhibited superior performance in UV-C for Rhodamine B degradation, diminishing under UV-A, attributed to nanoparticle agglomeration. ZnO and Ga:ZnO catalysts showed optimal performance under green light irradiation, highlighting their performances over the commercial zinc oxide material. Photoluminescence measurements suggested favorable gallium dopant incorporation, with no substantial variation of oxygen vacancies, consequently retaining the photocatalytic properties of ZnO, crucial for Rhodamine B degradation under green light irradiation. This study elucidates the intricate relationship between gallium doping, material properties, and photocatalytic performance, providing valuable insights for developing advanced photocatalysts.

INTRODUCTION

The water crisis has become a matter of supreme importance as our existence relies on it. Consequently, there is an urgent need to develop technologies that enhance the quality of reusable water and effectively mitigate the contamination that poses a significant risk to human,

animal, and environmental well-being.[1,2] In recent years, there has been a notable increase in the focus on advanced oxidation processes (AOP) to address the issue of water effluent contamination.[3] Among the different AOPs, heterogeneous photocatalysis offers several advantages compared to commonly employed approaches for removing synthetic organic dyes.[4,5] This environmentally friendly method utilizes sunlight or UV-visible irradiating lamps to initiate the degradation process by generating highly reactive oxygen species (ROS) that act as powerful agents to degrade a broad spectrum of toxic pollutants into harmless compounds and even mineralize them into carbon dioxide and water.[6]

Researchers have extensively explored various semiconductors in pursuit of this objective, with zinc oxide (ZnO) being an extensively studied material in the degradation of organic pollutants.[7–10] However, a notable limitation of zinc oxide is its predominant light absorption in the ultraviolet range of the solar spectrum, restricting its potential applications. To address this challenge, efforts have focused on modifying the morphological (based on their dimensions: 1D, 2D and 3D),[11] optical and structural properties (defect engineering, doping) of ZnO-based semiconductors to enhance light absorption and harness the entire solar spectrum.[12–14] Notably, the properties of pure n-type ZnO can be altered by introducing post-transition metal elements like Aluminum (Al), Gallium (Ga), and Indium (In).[15] Incorporating these post-transition metal ions induces the formation of defects, which generate mid-bandgap energy levels capable of increasing the ability to absorb photons in the visible range.[16] The radius of the trivalent dopant ions in CN=4 coordination In^{3+} (0.62 Å) > Ga^{3+} (0.47Å) > Al^{3+} (0.39 Å) compared to the Zn^{2+} ion (0.60 Å) facilitates the doping process, enabling more favorable lattice substitution. [17,18]

Given that aluminum has been extensively studied as a dopant and indium is both costly and challenging to procure, we opted in this study to explore the use of gallium as a dopant,

motivated as well by the limited body of research available on the photocatalytic activity of gallium-doped ZnO nanomaterials.

Due to their high electrical conductivity, surface area, and transparency, Ga-doped ZnO materials are ideal candidates for solar cells, smart windows, transparent conductive films for touch screens, gas sensing and light-emitting diodes (LEDs).[19–26] Additionally, ZnO nanomaterials containing gallium exhibit excellent light absorption properties, making them suitable for photocatalytic and environmental applications.[27–29]

In a photodegradation process, the photocatalytic activity of the material is strongly dependent upon the capability of the photocatalyst to generate electron (e^-)-hole (h^+) pairs and preventing recombination.[30] This results in the formation of free, highly reactive radicals such as hydroxyl radicals (•OH), which are able to oxidize organic molecules to initiate a degradation process.[31,32] The addition of Ga^{3+} into the zinc oxide matrix alters its electronic structure, facilitating the production (upon illumination) of electron-hole pairs, ultimately leading to the formation of active oxygen species,[33] a crucial step in the breakdown of organic dyes via oxidative mechanisms.

Ga-doped ZnO material is evaluated alongside its non-doped counterparts, pure zinc oxide and pure gallium oxide (Ga_2O_3), to investigate further the catalytic efficiency of ZnO influenced by gallium. This approach enables us to understand the role of gallium in catalytic processes and elucidate the contributions that gallium oxide might offer. In doing so, we aim to gain comprehensive insights into the influence of gallium in altering the host electronic structure and ability to generate electron-hole pairs – a fundamental factor in the photodegradation process.

Furthermore, it is important to acknowledge the existence of five different polymorphs of gallium oxide, named α-Ga_2O_3 (rhombohedral), β-Ga_2O_3 (monoclinic), γ-Ga_2O_3 (defective spinel), δ-Ga_2O_3 (cubic), and ε-Ga_2O_3 (orthorhombic), with α-Ga_2O_3 and β-Ga_2O_3 the most

common polymorphs.[34] The β-Ga_2O_3 is the thermodynamically stable polymorph under ambient conditions;[35] the other four polymorphs can be converted into β-Ga_2O_3 under certain circumstances and high temperatures.[36] While there is almost no information about the γ, δ and ε-phases, the other two are well studied for their electronic and optical properties as u-TCO (ultraviolet Transparent Conducting Oxide),[37,38] solar cells,[39] and phase shift masks for laser lithography.[40] In recent years, nanostructures composed of gallium oxide have emerged as promising materials for applications in wastewater treatment due to their electronic, catalytic, and optical properties.[41] Notably, Ghodsi et al. highlighted the superior catalytic properties of γ-Ga_2O_3 compared to β-Ga_2O_3 in the degradation of water pollutant dyes.[42] The researchers attributed this discrepancy in catalytic activity to variations in the occupancy of gallium ions between octahedral and tetrahedral sites, as well as distinct hybridization patterns with the surrounding oxygen ligands. In the literature, it is reported that γ-Ga_2O_3 has a defective-spinel-type structure, with partial occupancy of both tetrahedral and octahedral sites with a ratio of 0.85:1.15.[43,44] On the contrary, the β-phase has a 1:1 ratio with an equal occupancy of the tetrahedral (GaO_4) and octahedral (GaO_6) sites.[45] When transitioning from pure gallium oxide to gallium used as a dopant in the zinc oxide structure, the positions occupied by Ga^{3+} ions are influenced by the host matrix. In the wurtzite phase of zinc oxide, which features a hexagonally closed-packed arrangement of O^{2-} atoms, half of the tetrahedral sites are filled with Zn^{2+} ions, while the remaining tetrahedral sites and all octahedral sites are unoccupied.[46] Gallium ions can occupy the empty octahedral and tetrahedral sites, as well as substitute zinc ions. In fact, Ga^{3+} exhibits the advantage of having a comparable ionic radius (0.47 Å) to Zn^{2+} (0.60 Å). Consequently, substituting Ga^{3+} for Zn^{2+} in the ZnO lattice might cause minimal distortion and reduces the likelihood of observing undesirable secondary phases.[47]

Building on the promising prospects of Ga-doped ZnO, our research investigates how different gallium concentrations impact the ZnO properties using a straightforward solvothermal method.

Our ultimate goal is to synthesize quasi-spherical nanoparticles and investigate their photocatalytic performance, focusing on unravelling and comprehending the intricacies of the photocatalytic degradation process. This latter approach can be effectively applied to a broad spectrum of synthetic organic dyes, including Rhodamine B (RhB), selected as a target compound in this study. To the best of our knowledge, there is limited existing research on the photodegradation of Rhodamine B dye when exposed to Ga-doped ZnO materials under UV-visible light irradiation.[33,48,49] By studying the effect of different gallium doping levels in ZnO on the degradation of Rhodamine B, we aspire to gain deeper insights into the role that gallium plays in shaping the performance of advanced photocatalytic materials.

EXPERIMENTAL SECTION

Materials. The chemical reagents used in the study were utilized without further purifications. Zinc acetylacetonate hydrate, ($Zn(acac)_2 \cdot xH_2O$, 99.995 m/m%) and gallium acetylacetonate, ($Ga(acac)_3$, 99.999 m/m%) were obtained from Aldrich. Benzylamine (purity 99%) and ethanol absolute (used for analysis) were obtained from Merck.

General Synthesis. To synthesize the materials, including undoped zinc oxide (ZnO), Ga-doped ZnO, and pure gallium oxide (Ga_2O_3), a previously published method was followed.[50] For the synthesis, 1 g of $Zn(acac)_2$ was used to produce pure ZnO nanoparticles. To synthesize Ga-doped ZnO nanoparticles (Ga:ZnOs), $Zn(acac)_2$ was combined with $Ga(acac)_3$ at concentrations from 0.5 mol% (Ga:ZnO-05) to 5 mol% (Ga:ZnO-5). For pure Ga_2O_3 nanomaterial synthesis, 1 g of $Ga(acac)_3$ was employed.

Characterization methods. The Ga/Zn ratio in the powders was determined by inductively-coupled plasma optical emission spectrometry (ICP-OES, Perkin Elmer Optima 3300 DV simultaneous spectrometer, PerkinElmer, Waltham, MA, USA). To analyze the Zn and Ga content, a small portion of the Ga:ZnO sample was dissolved in a 5% aqueous nitric acid

solution (HNO_3, 69.0–70.0%, J.T.Baker, for trace metal analysis). The Ga:ZnO aqueous stock solutions and 1000 ppm Zn, Ga standards (Merck) were diluted by 5% HNO_3 to 1–10 ppm and 10, 5, 2 and 1 ppm concentrations, respectively, for ICP-OES measurements. All ICP measurements were carried out three times. The measurement error was evaluated based on calibration certificates and from statistical analysis of repeated measurements. Powder X-Ray Diffraction (PXRD) patterns were collected on a Panalytical X'Pert PRO multipurpose diffractometer (Cu Kα radiation, Bragg-Brentano geometry, X'Celerator linear detector). The undoped and Ga-doped ZnO powders were scanned between $2\theta = 10°$ and 70° with a 2θ scan step size of 0.0167°. Metal sample holders were used as a support for all powder samples. The profile analysis of the related diffraction patterns was carried out with the program DIFFRAC.EVA (general profile and structure analysis software for powder diffraction data, Bruker Analytical X-ray Systems).

Particle size and shape analysis was conducted using transmission electron microscopy (TEM) on a Tecnai 10 at an acceleration voltage of 100 kV. High Resolution TEM was performed on a Tecnai 20 for one selected sample. The sample was prepared by dispersing a small amount of powder in absolute ethanol, followed by deposition on a carbon-film-coated copper mesh, and drying. The particle size distribution was estimated based on 300 nanoparticles per sample. Fourier-transform infrared spectroscopy was performed on an FT-IR Bruker Vertex 70 FT-IR spectrometer. The transmittance of the KBr pellets containing the catalysts was measured at intervals of 4000-400 cm^{-1}. The discoloration process was monitored utilizing an Agilent Cary 5000 UV-VIS spectrophotometer. The measurements were carried out in the UV-visible 200-800 nm range, applying baseline corrections. ^{71}Ga magic angle spinning (MAS) solid-state NMR spectra were recorded at room temperature on a JEOL ECZ-R spectrometer operating at 14.1 T using a 3.2 mm Automas probe. The samples were packed in zirconia rotors and spun at 15 or 20 kHz. The spectra of Ga:ZnO samples were typically carried out using a Hahn echo

sequence and the following acquisition parameters: a relaxation time of 0.1 s, an excitation of 1.65 μs (90°), an acquisition time of 1.28 ms, and 300000 transients. The pre-echo and post-echo delays were equal to 50 and 28 us, respectively (spinning frequency = 20 kHz), or 75 μs and 53 μs (spinning frequency = 15 kHz). Data processing included multiplication of the FID (Free Induction Decay) by a line broadening factor of 20 Hz, zero-filling, Fourier transformation and phase corrections. The chemical shift scale was calibrated at room temperature using $Ga(NO_3)_3$ as the reference compound (0.0 ppm); see **Figure S4a** in **supporting information**. UV-Vis-NIR solid-state absorbance and transmittance spectra were collected (applying baseline corrections) on a Jasco V-750 spectrophotometer with a spectral bandwidth of 2 nm in the 200-800 nm range. Three-dimensional fluorescence mapping of samples was performed using a spectrofluorometer, a Jasco FP-8050, with a 450 W Xenon lamp as the excitation source. The maps were collected with an excitation range of 240–500 nm and an emission range of 300–700 nm with a 5 nm spectral bandwidth for excitation and emission. Photoluminescence measurements were performed in backscattering geometry with a confocal micro-Raman system (SOL Confotec MR750) equipped with a Nikon Eclipse Ni microscope. Samples were excited with 405 and 532 nm laser diodes (IO Match-Box series), and the spectral resolution was 0.6 cm^{-1} (average acquisition time 1 s, average number of acquisitions 3, sensor temperature −23 °C, objective Olympus 10×, grating with 150 grooves/mm, power excitation 3 mW).

The photocatalysts were assessed for their catalytic performance using UV-visible light exposure to measure the degradation of Rhodamine B, the representative dye compound. For conducting the photocatalytic experiments, a pair of custom-made photoreactors were employed.[50]

Photodegradation in the UV range. To conduct the photodegradation experiments, 20 mL of an aqueous solution of Rhodamine B with a concentration of 4 ppm was placed in quartz

beakers along with 5 mg of the photocatalyst. The experimental setup included a lamp emitting UV light, either UV-C (Osram Hg lamp, 11 W, dominant wavelength 254 nm) or UV-A (Philips Hg lamp, 11 W, dominant wavelength 368 nm), positioned centrally among the four beakers at a distance of 1 cm from the magnetic stirrer plate.[50] The reactor's temperature was maintained at room temperature (25 ± 3 °C) using a fan located on the back wall. Prior to irradiation, the reaction mixtures were stirred in the dark with a magnetic stirrer bar of equal length for 30 minutes to achieve substrate adsorption-desorption equilibrium. After 20 minutes of irradiation, the reactions were terminated. The suspensions were then centrifugated to separate the catalysts from the aqueous dye solution. Analysis was performed using UV-visible spectroscopy, specifically focusing on the primary absorption peak of the dye in the visible range at 554 nm. The percentage of degradation was calculated using **Formula (1)**.

$$\textbf{Degradation}\ \% = \frac{(A_0 - A)}{A_0} * \mathbf{100}, \qquad (1)$$

Where A_0 is the absorbance of the starting solution before irradiation, and A is the final absorbance measured after irradiation.

To evaluate the photocatalytic activity, experiments without the catalyst were also performed, exposing RhB dye uniquely to UV-C and UV-A light. In the absence of a photocatalyst, Rhodamine B degradation (%) was minimal under UV-C light (6 ± 3) and slightly higher under UV-A light (11 ± 1).

Photodegradation in the visible range. To conduct the photodegradation tests, a quartz beaker containing 20 mL of an aqueous solution of RhB with a concentration of 4 ppm and 5 mg of the photocatalyst was utilized. A visible light lamp with a dominant wavelength of 525 nm and power output of 18 W (Evoluchem LED) was positioned centrally, maintaining a distance of 10 cm from the top of the beaker. To prevent the contribution of UV-A light, a 405 nm long-pass edge filter (Semrock) was inserted between the beaker and the lamp. The reactor was maintained at room temperature (25 ± 2 °C) with the aid of a fan placed a few centimeters away

from the beaker within the reactor. Before irradiation, the reaction mixtures were stirred in the dark for 30 minutes using a magnetic stirrer bar of equal length to establish substrate adsorption-desorption equilibrium. After 60 minutes of irradiation, the reactions were terminated. The suspensions were then subjected to centrifugation to separate the catalysts from the dye solution. Analysis was performed using UV-visible spectroscopy, focusing on the primary absorption peak of the dye in the visible range at 554 nm. We conducted experiments without the catalyst to assess photocatalytic activity, subjecting RhB dye exclusively to visible light to gauge its susceptibility.[51] Without a photocatalyst, Rhodamine B degradation under green light exposure was minimal. Our prior study reported approximately 5% degradation after one hour of green-light exposure.[50] However, the dye-catalyst suspension did experience discoloration under green light irradiation. To ensure measurement reliability, the photocatalytic irradiation experiments were repeated three times for data reproducibility. The percentage of degradation was calculated using **Formula (1)**.

RESULTS AND DISCUSSION

The main focus of this study is to investigate the impact of varying gallium dopant percentages (0%, 0.5%, 1%, 2%, 3%, 4% and 5%) on ZnO nanoparticles.

Various analytical techniques, including powder X-ray diffraction (PXRD), inductively coupled plasma-optical emission spectrometry (ICP-OES), transmission electron microscopy (TEM), Fourier transform infrared (FT-IR), Nuclear magnetic resonance (NMR) spectroscopy, Solid-state UV-Vis, and Photoluminescence (PL) analyses were performed to investigate and evaluate potential effects of gallium doping on the zinc oxide structure; which will be further explored for their photocatalytic activity in degrading Rhodamine B dye under UV-Visible light exposure. The resulting synthesized and commercially obtained samples are categorized and listed in **Table 1**.

Table 1. Commercial, undoped zinc oxide, Ga-doped ZnO and pure gallium oxide sample codes. Nominal and experimental percentage of gallium content into the as-synthesized Ga-doped ZnO solids.

Sample Type	Sample Code	Nominal Ga content (%)	Experimental Ga content (%)
Commercial ZnO	CZnO	-	-
Undoped ZnO	ZnO	-	-
Ga-doped ZnO	Ga:ZnO-05	0.50	0.44
Ga-doped ZnO	Ga:ZnO-1	1.00	0.88
Ga-doped ZnO	Ga:ZnO-2	2.00	1.73
Ga-doped ZnO	Ga:ZnO-3	3.00	2.54
Ga-doped ZnO	Ga:ZnO-4	4.00	3.30
Ga-doped ZnO	Ga:ZnO-5	5.00	3.65
Pure as-synthesized γ-Ga_2O_3	γ-Ga_2O_3	100	100
Commercial β-Ga_2O_3	β-Ga_2O_3	100	100

To quantitatively evaluate the amount of gallium dopant incorporated within the ZnO structure, ICP analyses were performed on the Ga:ZnO materials, see **Table 1**.

While the existence of an additional phase (vide infra) could potentially introduce inaccuracies in the compositional analysis, the findings reveal a positive correlation between the nominal quantities of gallium introduced in the synthesis mixture and the gallium content observed in the eventual solid product. The results agree with the literature[24] from which it is clear that incorporating the dopant into the zinc oxide lattice is more effective when the Ga/Zn ratio is

lower than 2 at% with respect to Zn. The missing gallium was likely eliminated through the repeated washing steps.

Transmission electron microscopy was employed to assess the morphology and size of the synthesized materials. Both the undoped and Ga-doped ZnO powders exhibited quasi-spherical shaped nanoparticles, as depicted in **Figure 1** and **Figure S1a** in **supporting information**. As displayed by the micrographs, the different gallium dopant contents do not lead to any significant changes in the size of the nanoparticles; see histograms in **Figure S2** in **supporting information**. They exhibited average diameters between 5 and 80 nm. **Figure S1** also displays the TEM image of the as-synthesized γ-Ga_2O_3. The particle size distribution shows a diameter lower than 10 nm, indicating the production of very small nanoparticles. The absence of stabilizing surfactants in all the synthesized materials results in an aggregation propensity. This process is more evident for the pure as-synthesized γ-Ga_2O_3 phase nanoparticles that are distinguishable from each other. To have a complete overview, TEM images of commercial β-Ga_2O_3 and commercial zinc oxide (CZnO) are displayed in **Figure S1c, d** in **supporting information**.

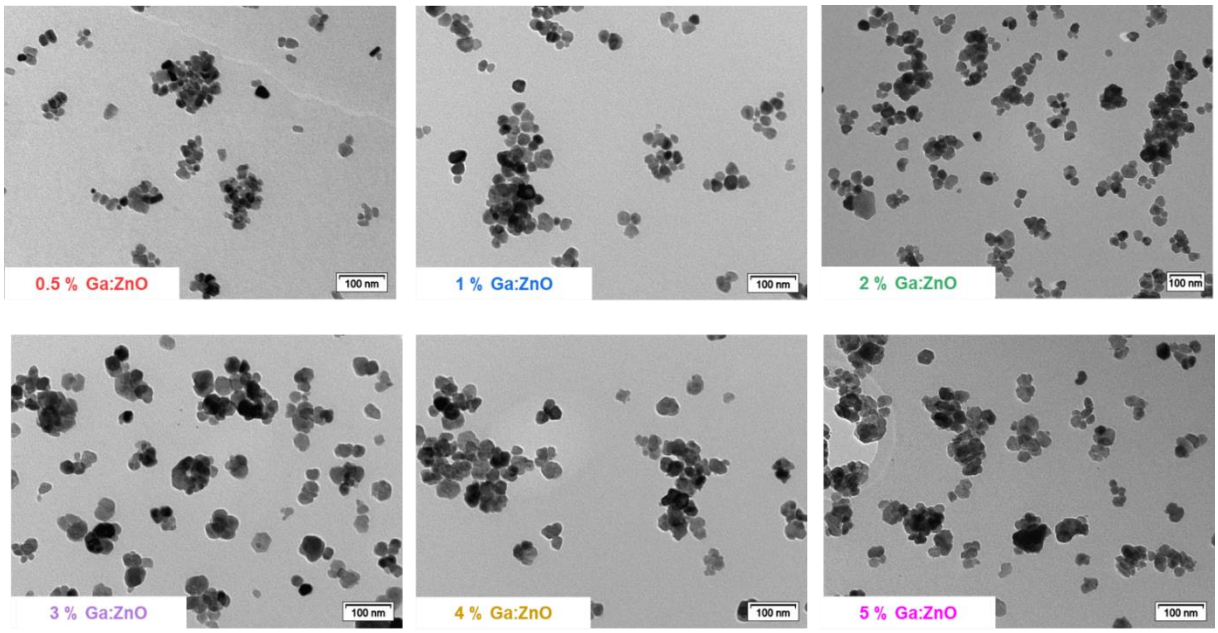

Figure 1. TEM micrographs of the Ga-doped ZnO from Ga:ZnO-05 to Ga:ZnO-5 as-synthesized materials.

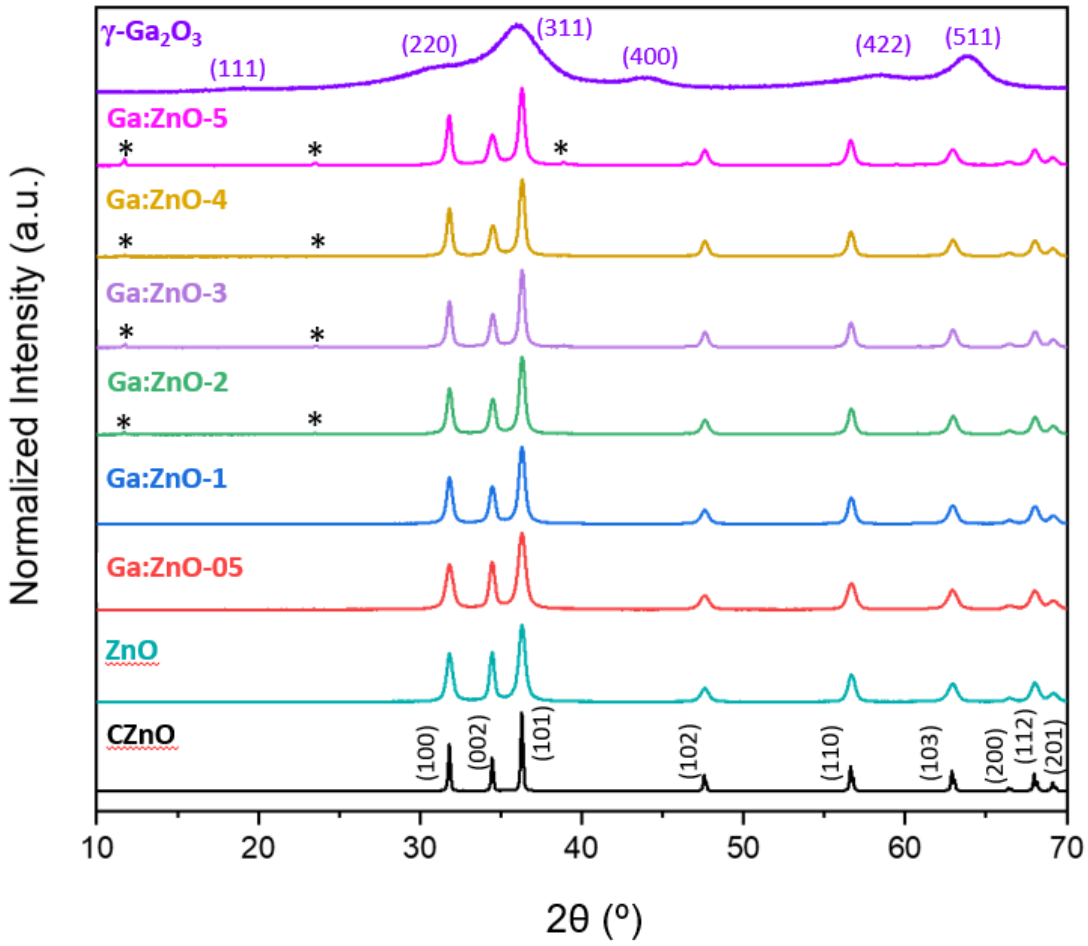

Figure 2. Powder X-ray diffraction patterns of commercial ZnO, and as-synthesized undoped ZnO, Ga-doped ZnO with variant gallium content and pure γ-gallium oxide nanomaterials. Commercial zinc oxide is used as reference material for the samples containing zinc oxide. Symbol: *-corresponds to the secondary phase Zinc gallium carbonate LDH.

To acquire further insights into the structure of the nanomaterials, powder XRD patterns of commercial ZnO, undoped ZnO, Ga-doped ZnO, and pure as-synthesized gallium oxide were acquired. Commercial zinc oxide was used as a reference solid. The diffractograms are presented in **Figure 2**.

The patterns of commercial zinc oxide and as-synthesized zinc oxide material are well-matched with the hexagonal wurtzite crystal phase (PDF card 89-1397). The characteristic diffraction peaks 2 θ = 31.80º, 34.45º, 36.27º, 47.57º, 56.64º, 62.90º, 66.45º, 68.03º and 69.15º indicate the reflections from the (100), (002), (101), (102), (110), (103), (200), (112) and (201) crystal planes, respectively. For the Ga-doped ZnO samples with up to 1% of gallium content, the corresponding patterns merely show the undoped ZnO phase; thus, suggesting either a complete incorporation of the dopant into the zinc oxide lattice or formation of a secondary phase with a concentration below the detection limit of the instrument. For the nanomaterials with a nominal gallium content varying from 2 to 5%, an additional crystalline phase, identified as Zinc gallium carbonate LDH (245124-ICSD),[52] is observed. Although the Ga^{3+} ion (0.47 Å) is smaller than the Zn^{2+} ion (0.60 Å), its incorporation is complex, and it can continue until the doping concentration surpasses the solubility limit of the host matrix, as already reported in the literature.[26] Therefore, a segregated phase of gallium atoms external to the ZnO lattice is formed beyond this solubility limit. As indicated by the PXRD in **Figure 2**, following the ICP results in **Table 1**, when the Ga/Zn doping ratio is higher than 1 at%, a portion of gallium is not introduced into the ZnO lattice, part of it forming a segregated phase external to the zinc oxide lattice.

Figure 2 also displays the PXRD pattern of pure as-synthesized gallium oxide that is well-matched with the 236276-ICSD card that infers the information of γ-Ga_2O_3 with the defective spinel cubic crystal structure. The characteristic broadened diffraction peaks 2θ = 18.68º, 30.86º, 36.10º, 43.85º, 58.25º, 63.98º correspond to the (111), (220), (311), (400), (422), and (511) reflections, respectively. The PXRD analysis of the commercial gallium oxide β-phase (34243-ICSD) is also reported as a standard reference in **Figure S3** in **supporting information**. Contrary to the sharp lines of the other materials reported in **Figure 2** and **Figure S3**, all the

diffraction peaks of the as-synthesized γ-gallium oxide are broad and, in accordance with the TEM images in **Figure S1b** in **supporting information**, it is nanosized particles.

Motivated by the intention to explore the structural properties of our synthesized materials at a local level, solid-state ^{71}Ga NMR spectroscopy was utilized, see **Figure 3** and **Figure S4** in **supporting information**.

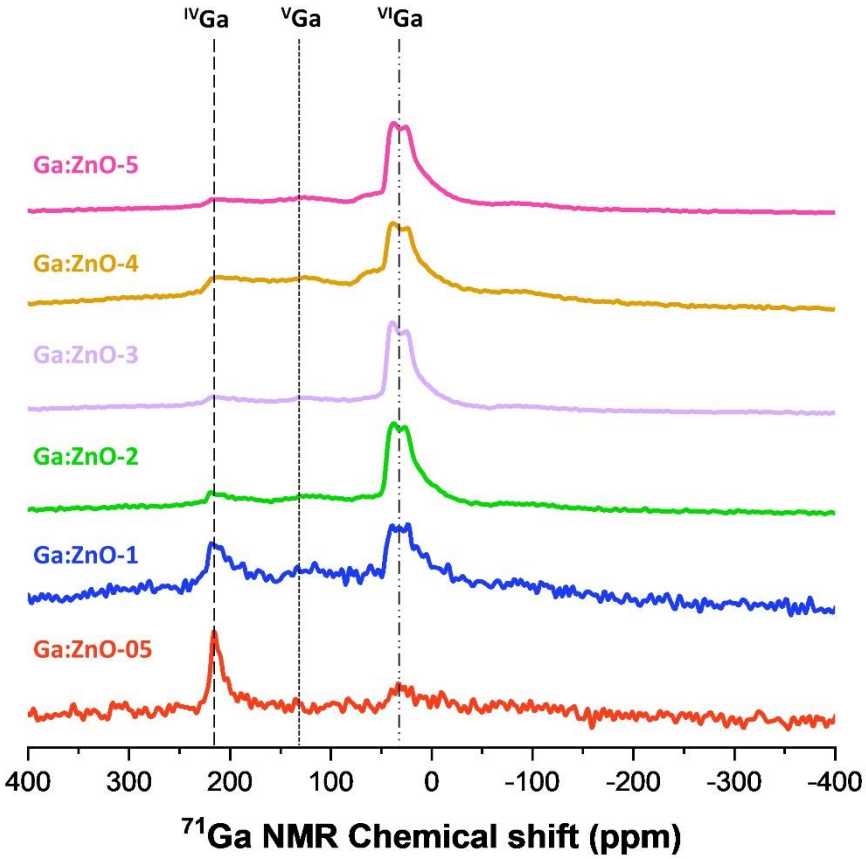

Figure 3. ^{71}Ga MAS NMR of Ga:ZnO nanoparticles as-synthesized with a different nominal gallium content. The lines highlight the peaks assigned to the 6−fold coordinated gallium, ^{VI}Ga, 4−fold coordinated gallium, ^{IV}Ga, and 5−fold coordinated gallium, ^{V}Ga.

Solid-state NMR spectroscopy is a valuable tool for studying gallium coordination in both crystalline and amorphous materials. Gallium has two NMR active nuclei, ^{69}Ga and ^{71}Ga, both with nuclear spin of I = 3/2 and natural abundances of 60.1% and 39.9%, respectively.[53] Despite

lower natural abundance, ^{71}Ga is generally chosen over ^{69}Ga due to its lower electric quadrupole moment and slightly higher sensitivity.[54] It is challenging to obtain direct structural information from amorphous samples, as the signals would result from a distribution of quadrupolar couplings constants (CQ), and the dominant signals would be associated with smaller CQ values. Magic angle spinning (MAS) NMR experiments were conducted at 20 kHz and a magnetic field of 14.1 T to examine the gallium coordination. The ^{71}Ga NMR spectra of the as-synthesized γ-Ga_2O_3 and the commercial β-Ga_2O_3 are shown and discussed in **supporting information**; see **Figures S4b**, **e** and **f**.

To explicitly refer to the coordination number of gallium and avoid confusion with the oxidation state, in this work, the notations ^{VI}Ga, ^{V}Ga and ^{IV}Ga have been adopted, where the Roman numerals indicate the number of coordinating oxygen atoms rather than the oxidation state of gallium.

The ^{71}Ga-NMR spectra in **Figure 3** displayed multiple asymmetric resonance lines: the 6-fold coordination signal between 0-50 ppm corresponds to gallium coordinated to 6 oxygen atoms (octahedral, ^{VI}Ga)[53] together with its spinning sidebands at about - 109 ppm (see **Figure S4d** in **supporting information**). The signal observed around 200 ppm is typical for gallium in 4-fold coordination with oxygen atoms (tetrahedral, ^{VI}Ga). The signal around 140 ppm might indicate the presence of gallium in a distorted 4-fold coordination state, ^{V}Ga (see **Figure S4c** in **supporting information**).[55,56]

Analysis of the ^{71}Ga-NMR data revealed that incorporating a small amount of gallium into the zinc oxide lattice primarily occurs in tetrahedral sites (see **Figure 3**, Ga:ZnO-05). At increasing amounts of gallium (see spectra of Ga:ZnO-1 to Ga:ZnO-5), the insertion of gallium atoms occurs mainly in octahedral sites (^{VI}Ga). In the samples with 2-5% gallium, distorted tetrahedral sites (^{V}Ga) and ^{IV}Ga signals have similar intensities.

The substitution of Zn^{2+} ions with Ga^{3+} ions introduces excess positive charges.[57,58] It is plausible that the signal attributed to tetrahedral gallium arises from Ga^{3+} ions occupying vacant tetrahedral positions rather than directly replacing Zn^{2+} ions. Existing literature indicates that gallium ions can occupy both substitutional and interstitial sites within the zinc oxide lattice.[59]

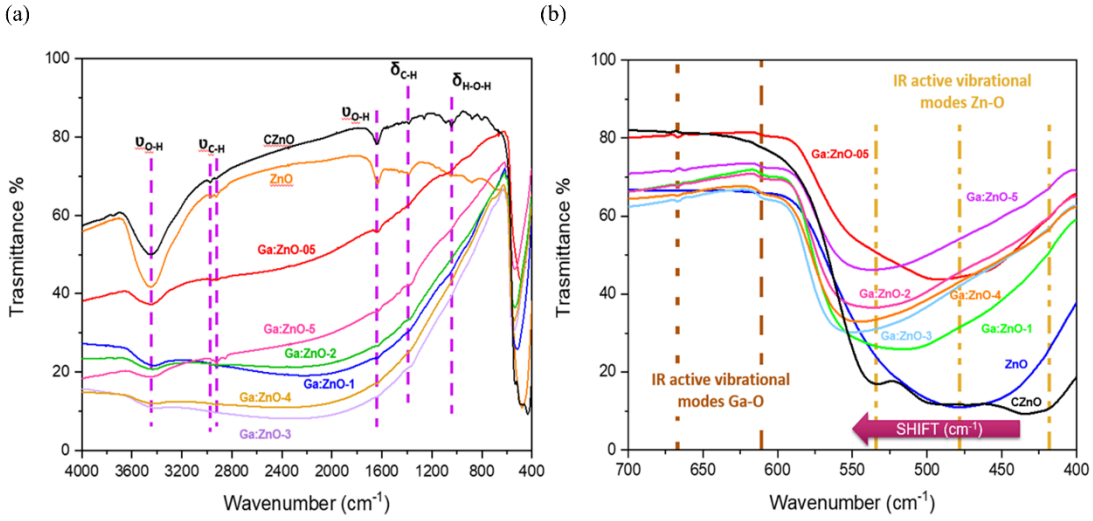

Figure 4. FT-IR spectra of CZnO, ZnO, and Ga:ZnO series in function of the nominal Ga content, (a). Magnification of part of the fingerprint region, (b).

Infrared measurements assessed the possible substitution of the Zn^{2+} with the dopant ions. The FT-IR technique is used to i) obtain information about the vibrational stretching and bending of the metal-oxygen bond in oxide nanomaterials, ii) identify impurities, iii) reveal the dopant incorporation through the localized surface plasmon resonance (LSPR)[60] and iv) to identify the chemisorbed molecules on the surface of the nanoparticles. The transmittance of the KBr pellets containing CZnO, ZnO, Ga:ZnO, γ-Ga_2O_3 and β-Ga_2O_3 materials was measured in the interval of 4000–400 cm^{-1}; see **Figure 4** and **Figure S5** in **supporting information**.

The region between 400–700 cm^{-1} illustrates the infrared vibrational active modes of Zn-O bonds in zinc oxide at ca. 418, 480 and 534 cm^{-1}; see **Figure 4a, b**.[26,61,62] In the latter figure,

two lines highlight the absorption peaks at ca. 610 and 667 cm^{-1}. These two are ascribed to the vibrational modes of Ga-O bonds.[63] The bands at ca. 3450, 1637 and 1045 cm^{-1} are related to the stretching and bending modes of O-H groups in physisorbed water.[29] The peaks observed at ca. 2970, 2921, and 1375 cm^{-1} are due to C-H stretching (asymmetric and symmetric) and bending vibrations of alkane groups.[64] These are ascribed to impurities present in the KBr powder. In addition to these peaks, a distinct band spanning from 800 to 3000 cm^{-1} is prominently observed in the Ga:ZnO samples, while it is absent in the undoped materials. This band, known as the Localized Surface Plasmon Resonance (LSPR) band, is a distinctive feature of n-doping in the Ga:ZnO nanoparticles, attributable to the increased density of free electrons. The position of the LSPR band depends on carrier concentration, carrier mobility, defects and other parameters.[65] As discussed in our previous work concerning the doping with aluminium,[50] the insertion of the Al^{3+} as well as the Ga^{3+} dopant leads to a displacement of the Zn^{2+} into the oxide lattice with consequent change in peak shape and shift towards higher wavenumbers, as shown in **Figure 4b**.

In **Figure S5** are displayed the FT-IR spectra of commercial β-Ga_2O_3 and as-synthesized γ-Ga_2O_3 materials. The commercial β-Ga_2O_3 material is used as a reference. The broad absorption signal in the FT-IR spectrum at 3450 cm^{-1} corresponds to the O-H stretching vibration, and the signal at ca.1633 cm^{-1} corresponds to the H-O-H bend vibrations of adsorbed water, as previously shown in **Figure 4a**. The peaks observed at ca. 472, 493, and 669 cm^{-1} are infrared active optical phonon modes vibrations from the Ga-O bonds.[66–71] An extra peak is observed for the β-phase at ca. 754 cm^{-1}, corresponding to the vibrations of Ga-O in GaO_4.[72] Additionally, as previously observed, the bands displayed at ca. 2958, 2921, and 1380 cm^{-1} are due to C-H asymmetric stretching and bending vibrations of alkane groups, impurities in KBr used to make the FT-IR pellets.

Photocatalytic degradation of Rhodamine B dye

Building upon the characterization outlined earlier, our focus in the following discussion will center on four distinct nanomaterials, namely ZnO, Ga:ZnO-05, Ga:ZnO-5, and γ-Ga_2O_3, chosen for their different properties. Specifically, we delve into the characteristics of pure as-synthesized zinc oxide and gallium oxide, along with their counterparts representing 0.5% and 5% gallium-doped zinc oxide. This selection encapsulates the broader spectrum of gallium-doped variants. The photocatalytic activity of the selected solids was evaluated by monitoring the decolorization of Rhodamine B dye suspensions under UV-green light exposure. After removal of the solid catalyst (when needed), the degradation of the RhB dye was confirmed by analyzing the UV-vis spectrum of the dye solution.

The general mechanism of Rhodamine B degradation in the presence of photocatalysts under UV-visible light irradiation has been extensively reported in the literature.[73–77] However, in this study, the primary objective was to evaluate the photocatalytic activity of the synthesized materials rather than to investigate the detailed degradation pathway of RhB itself.

Table 2. Photodegradation of RhB under UV-C, UV-A (20 min duration) and green light irradiation (60 min duration) in the presence of commercial ZnO (CZnO), undoped-ZnO (ZnO), γ-Ga_2O_3, commercial β-Ga_2O_3, and 0.5 and 5 at% Ga-doped ZnO nanopowders (Ga:ZnO-05 and Ga:ZnO-5). RhB photolysis tests under UV-C, UV-A and green light irradiation.

		Rhodamine B Dye Photodegradation [%]		
Entry	**Sample code**	**UV-C 254 nm**	**UV-A 368 nm**	**Green light 525 nm**
1	CZnO	94 ± 1	95.9 ± 0.1	20 ± 4
2	ZnO	44.6 ± 0.5	70 ± 3	39 ± 1

3	Ga:ZnO-05	45± 3	28 ± 5	36 ± 2
4	Ga:ZnO-5	34 ± 1	26 ± 3	36 ± 1
5	γ-Ga_2O_3	71 ± 3	9 ± 2	ND
6	β-Ga_2O_3	97.7 ± 0.5	6 ± 2	ND
7	RhB without catalyst	6 ± 3	11 ± 1	5.2 ± 0.1

Table 2 displays the photocatalytic activity in terms of dye degradation (%) of commercial ZnO, as-synthesized undoped-ZnO, Ga-doped ZnO (with different percentages of gallium), γ-Ga_2O_3 and commercial β-Ga_2O_3 nanomaterials. The undoped zinc oxide and the γ-Ga_2O_3 materials were used to complete the Ga-doped ZnO series. The commercial zinc oxide and commercial gallium oxide were evaluated as references.

Adsorption experiments in the dark were conducted on commercial zinc oxide and as-synthesized undoped-ZnO, with adsorption values after one-hour under magnetic stirring of 15% and 10%, respectively. The activity was monitored after 20 minutes of irradiation under UV-C, UV-A, and after 60 minutes under green light. Under UV-C light irradiation, RhB degradation occurred in the presence of all catalysts. Notably, among the Ga:ZnO catalysts, the best photocatalytic performance is observed for Ga:ZnO-05 (entry 3), equivalent to the photocatalytic activity of undoped zinc oxide (entry 2). These results indicate a decrease in photocatalytic activity with increasing the gallium content in the catalyst. However, CZnO (entry 1), γ-Ga_2O_3 (entry 5) and β-Ga_2O_3 (entry 6) catalysts display superior photocatalytic activity under UV-C compared to as-synthesized ZnO (entry 2) and Ga:ZnO materials (entries 3,4). This behavior can be explained considering that their bandgaps lay in the UV light spectrum; see **Figure S6** in the **supporting information**. The decreased photocatalytic activity

of γ-Ga_2O_3 (entry 5) compared to β-Ga_2O_3 (entry 6), can be attributed to the pronounced tendency of nanoparticles in γ-Ga_2O_3 to aggregate, as evidenced in the TEM image presented in **supporting information**, **Figure S1b**. This aggregation phenomenon reduces the available surface area for photocatalysis, thereby diminishing performance under UV-C light irradiation. From UV-C to UV-A light irradiation, commercial zinc oxide (entry 1) performs best due to its bandgap value of 3.87 eV.50 The ZnO material (entry 2) increases its photocatalytic activity under UV-A because its bandgap lies between UV-A and the visible light spectrum.[50] The catalytic activity of γ-Ga_2O_3 (entry 5) and β-Ga_2O_3 (entry 6) drastically drops upon moving further away from their bandgap. The photocatalytic activity of Ga:ZnO materials (entries 3,4) also shows a decrease. This could be explained by the gallium dopant incorporated into the zinc oxide lattice, altering the structure and defects that originally enabled the undoped material to perform well under UV-A irradiation.

Table 2 also presents the RhB photodegradation data for a one-hour irradiation under green light (525 nm) for the CZnO (entry 1), ZnO (entry 2) and Ga:ZnO nanomaterials (entries 3,4). Notably, the 20% dye degradation observed with CZnO (entry 1), as detailed in **Table 2** and previously discussed in our earlier work,[50] might be linked to the thermal decomposition of the dye. This decomposition likely occurred due to continuous irradiation for one hour using a high-power lamp, along with the adsorption-desorption equilibrium experiment in the dark.

It is noteworthy that under green light exposure, the catalytic performance exhibited by undoped zinc oxide (entry 2) equals that of Ga:ZnO materials (entries 3,4), which demonstrate superior activity compared to CZnO (entry 1). A possible explanation might be related to the position occupied by gallium ions in the zinc oxide lattice and the defects that are consequently created due to the insertion of the dopant.

In contrast to our previous study,[50] which investigated the substitution of Zn^{2+} with Al^{3+}, where the performance of ZnO-based photocatalysts was adversely affected by the dopant

concentration; the present research focuses on materials synthesized using the same method but with a different dopant. Remarkably, in this context, the incorporation of gallium does not show any detrimental effects on the intrinsic photocatalytic activity.

In elucidating the photocatalytic behavior, the nanomaterials' optical properties were explored, yielding valuable insights into their structural defects. First, the focus is on the features of the γ-Ga_2O_3 defective-spinel nanomaterial compared to the ones of the commercial β-Ga_2O_3 sample. The optical absorption of the samples showed a very different trend of the reflectance spectra, with the commercial β-Ga_2O_3 mainly reflecting radiation above ca. 270 nm whilst the as-synthesized γ-Ga_2O_3 only partially reflected in the near UV region. These differences were highlighted by plotting the pseudo-absorption F(R∞) as a function of the absorbed photon energy to calculate the bandgap of these materials (**Figure S6**, details in **supporting information).** Commercial β-Ga_2O_3 presents the typical sigmoidal pattern whose fitting with a Boltzmann function results in a bandgap of about 4.7 eV in perfect agreement with the literature.[78–80]

On the other hand, γ-Ga_2O_3 sample shows an absorption curve that can be described as the overlap of a typical sigmoidal plot with a Gaussian band, indicating the presence of defects that enhance the absorption of the material in the near UV and visible region. Indeed, the bandgap value was closer to the commercial one (4.9 eV) with the addition of a Gaussian component peaked at about 4.2 eV (ca. 300 nm) and extending up to about 2.5 eV (ca. 500 nm). The presence of this change in the optical features was further investigated by measuring the photoluminescence at different excitation wavelengths (**Figure 5, Figure S7** in **supporting information**).

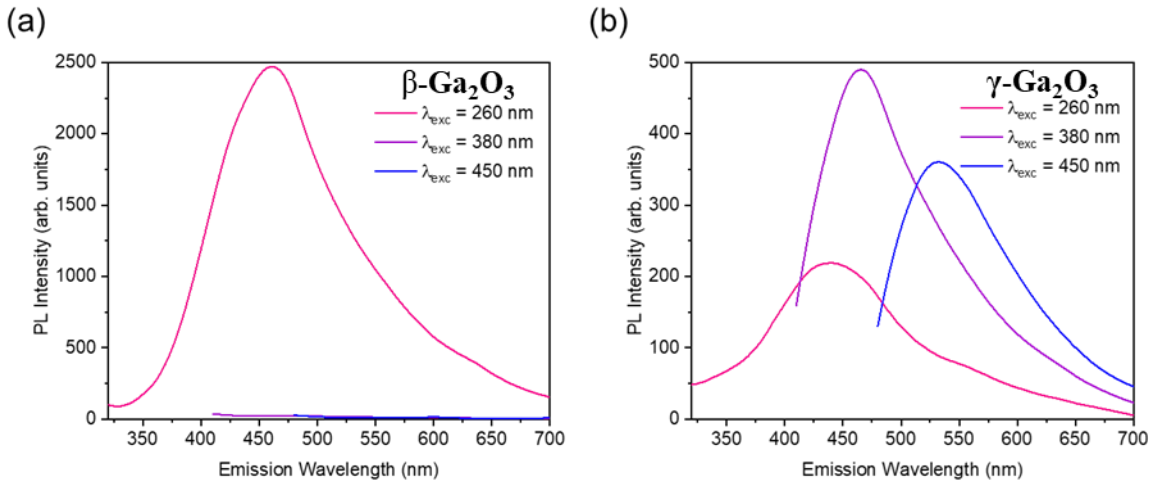

Figure 5. PL spectra excited at 260, 380 and 405 nm. Comparisons between commercial β-Ga_2O_3 (a) and as-synthesized γ-Ga_2O_3 (b).

PL spectra clearly show that commercial gallium oxide emits only under 260 nm irradiation, whilst our synthesized sample is photoluminescent also under 380 and 450 nm excitation, confirming its absorption features in the UV-visible range. Indeed, an excitation dependent emission in the 400-600 nm was recorded when excited in the 350-500 nm range (see excitation-emission maps in **supporting information**, **Figure S7**). Nevertheless, luminescence can act as a competitive phenomenon to the photocatalytic process due to the recombination of the electron-hole couple that, in this case, cannot be transferred to the material to activate the photocatalytic sites. This explanation fits well with the experimental findings on the photocatalytic performance of our synthesized γ-Ga_2O_3, whose best results are obtained under UV-C irradiation. This variation in the optical properties between the two types of gallium oxide materials could be linked to both the presence of structural defects (as suggested by the absorption band at 4.2 eV) and the nano-dimension of our sample, whose particles can be subjected to a quantum confinement effect that changes the emission properties according to the particle size distribution (see TEM image **Figure S1b** in **supporting information**).[81–83]

For what concern the optical properties of our as-synthesized ZnO, they have already been discussed in detail in our previous paper.[50] Indeed, our findings showed that our nanosized ZnO presents red-emitting centers under visible light irradiation that were ascribed to a high content of O_2^{2-}, which is the main initiator of the photodegradation and responsible for the discoloration of the RhB dye.[84]

Ga-doped ZnO photocatalysts were also studied through absorption and photoluminescence. UV-Vis reflectivity/absorption measurements of Ga:ZnO-05 and Ga:ZnO-5 samples show a slight variation that does not significantly change the bandgap value that was calculated for both samples to be about 3.2 eV, comparable with the value of the undoped ZnO (ca. 3.3 eV) (**Figure S8** in **supporting information**).

However, while both undoped and Ga-doped ZnO maintains a bandgap value similar to commercial ZnO, its visible light activity is not driven by direct bandgap transitions but instead by mid-bandgap defect states induced by our synthetic process. These sub-bandgap states enable light absorption in the infra-gap visible region, which explain the photocatalytically activity under green light irradiation. This explanation is supported by the steady-state PL spectroscopy, which allows a higher sensitivity to defect-related emissions over the optical absorption technique. Indeed, to bypass the high excitonic contribution that can cover possible defect emission signals, these measurements were carried out by exciting in the infra-gap visible region at 405 and 532 nm (**Figure 6** and **Figure S9** in **supporting information**, respectively). The irradiation was performed using laser beams of which the monochromatic emission and high power helped enhance our samples' low luminescent signal.

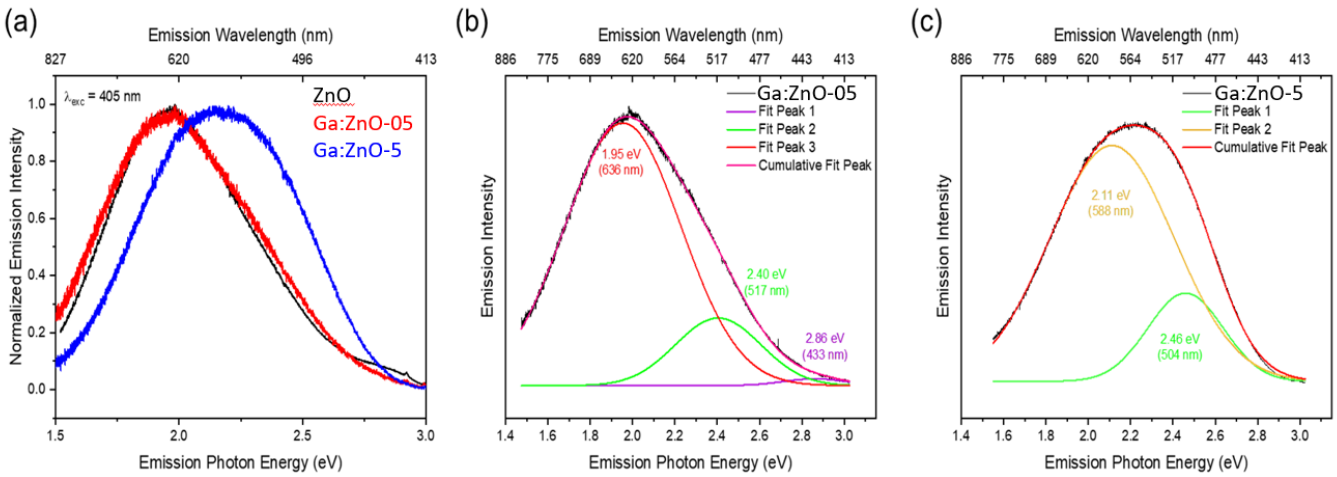

Figure 6. Emission spectra of ZnO, Ga:ZnO-05 and Ga:ZnO-5 acquired by exciting the samples at 405 nm (a). Gaussian deconvolution of the emission spectra acquired by exciting Ga:ZnO-05 (b) and Ga:ZnO-5 (c) with a wavelength of 405 nm.

By exciting the samples with 405 nm irradiation, we were able to confirm the presence of defects that absorbs in the visible range in every as-synthesized sample, observing broad emission bands, spanning from blue to orange, resulting from the overlap of these defect contributions. Indeed, Ga:ZnO-05 displayed a broad emission pattern very similar to the undoped sample (ZnO), with a slight increase in the relative contribution of the green emission. This emission profile was attributed to a convolution of various factors, including surface interstitial Zn (violet band), charged oxygen vacancies (green band), and photocatalytically active peroxide-like species[85] O_2^{2-} interacting with the ZnO surface (red band).[50] In the Ga:ZnO-5 sample, there's a notable shift in the red band, from approximately 635 nm to around 590 nm, indicating a blue-shift of the predominant emissive band. Meanwhile, the green band undergoes a minor red-shift, transitioning from 504 nm to 517 nm. The observed wavelength shifts, reported also for the largest Al-doped sample in our previous work, can be explained by the insertion of Ga^{3+} ions into zinc oxide, which alters the atomic environment and causes a shift of the designated bands.

Nevertheless, in opposition to our previous results, despite the increase in dopant content, the proportion of the green band associated with charged oxygen vacancies—known to reduce catalytic performance—remains relatively stable, shifting from 16% in Ga:ZnO-05 to 20% in Ga:ZnO-5. This observation is crucial in understanding the sustained photocatalytic performance of our Ga:ZnO samples under visible light, irrespective of the dopant concentration. Indeed, in our previous work,[50] we elucidated the photocatalytic behaviors of Al-doped ZnO nanomaterials under visible light irradiation, and the introduction of Al^{3+} ions into ZnO at a high doping level (nominal 5 at%) resulted in a decrease in photocatalytic efficiency. This decrease was attributed to the significant enhancement of the green emission contribution, accounting for up to 53%, associated with a higher presence of oxygen vacancies, which in turn hinders the photocatalytic activity. In contrast, this enhancement was not observed in the newly Ga-doped samples, confirming the restrained increase in oxygen vacancies and the preservation of O_2^{2-} species content that maintains the photocatalytic performance. Our observation that these properties do not change in the Ga-doped samples, is further corroborated by the measurements at 532 nm, for which only a tiny red shift is recorded in Ga:ZnO-05. Moreover, the excitation with green light further demonstrated the material's ability to absorb light in this region, which explains its photocatalytic activity under visible light.

It is worth noting that the origin of the photocatalytic activity of these samples was deduced through the analysis of the low efficient luminescence properties more than on the analysis of the bandgap of the material. Indeed, there is a correlation between bandgap redshift and increase of peroxide defects that enhance photocatalysis. However, while UV-Vis measurements reveal the general trend of defect formation, the deconvolution of PL emission spectra provides a more sensitive and detailed view of this correlation. PL spectroscopy allows us to probe defect-related emissions directly, making it a more effective technique for identifying the presence of defect states that contribute to the photocatalytic process.

CONCLUSIONS

This investigation into Ga-doped ZnO nanomaterials for the photodegradation of Rhodamine B dye in aqueous solution under UV-green light exposure provides valuable insights into the complex relationship between gallium doping, material properties, optical features, and photocatalytic activity. By systematically exploring the impact of gallium dopant concentration on structural, morphological, and optical properties, this research contributes to the optimization of photocatalytic materials designed for environmental remediation and other applications. Therefore, the correlation between defects, synthesis route, particle size, and photocatalytic activity is highlighted. Notably, even with structural alterations induced by gallium doping, Ga:ZnO nanoparticles maintain a comparable photocatalytic activity to undoped zinc oxide when exposed to green light. The latter underscores the significance of defect retention within Ga:ZnO nanomaterials. By elucidating the retention of defects associated with O_2^{2-} species in Ga:ZnO materials, this study demonstrates their ability for photocatalytic degradation of Rhodamine B under green light irradiation, emphasizing the significance of defect engineering in photocatalytic materials design. Furthermore, the investigation into the optical features and photoluminescence of Ga:ZnO materials reveals minimal differences in spectra between undoped ZnO and Ga:ZnO materials. This suggests that gallium doping, facilitated by the similar size of Ga^{3+} with Zn^{2+}, allows the preservation of photocatalytic properties in the doped-zinc oxide material under the study conditions.

ASSOCIATED CONTENT

Supporting Information. The supporting information is available at (….).

TEM images, particle size distribution histograms, XRD patterns, NMR spectra, FT-IR spectra, reflectance spectra, excitation-emission maps, photoluminescence spectra, Gaussian band deconvolution data, and calculated bandgaps of investigated materials (PDF).

AUTHOR INFORMATION

Corresponding Authors

* Carmela Aprile, University of Namur, Unit of Nanomaterials Chemistry, Department of Chemistry, NISM, Rue de Bruxelles, 61-5000 Namur, Belgium.

carmela.aprile@unamur.be

Author Contributions

The manuscript was written through the contributions of all authors. All authors have given approval to the final version of the manuscript.

Funding Sources

This research was co-funded by Hasselt University and Namur University through the BOF programme (Project R-9087) and the Fonds spécial de recherche. This work was further supported by Hasselt University and the Research Foundation Flanders (FWO Vlaanderen) via the Hercules project AUHL/15/2-GOH3816N. This study employed resources of the PC2 and the MORPH-IM platforms located at the University of Namur.

REFERENCES

(1) UNESCO World Water Assessment Programme. *Partnerships and Cooperation for Water*; 2023. https://doi.org/10.1016/B978-0-12-821057-4.00003-3.

(2) Salehi, M. Global Water Shortage and Potable Water Safety; Today's Concern and Tomorrow's Crisis. *Environ. Int.* **2022**, *158*, 106936. https://doi.org/10.1016/J.ENVINT.2021.106936.

(3) Kumari, P.; Kumar, A. ADVANCED OXIDATION PROCESS: A Remediation Technique for Organic and Non-Biodegradable Pollutant. *Results in Surfaces and Interfaces* **2023**, *11*, 100122. https://doi.org/10.1016/J.RSURFI.2023.100122.

(4) Byrne, C.; Subramanian, G.; Pillai, S. C. Recent Advances in Photocatalysis for Environmental Applications. *J. Environ. Chem. Eng.* **2018**, *6* (3), 3531–3555. https://doi.org/10.1016/j.jece.2017.07.080.

(5) Reddy, P. A. K.; Reddy, P. V. L.; Kwon, E.; Kim, K.-H.; Akter, T.; Kalagara, S. Recent Advances in Photocatalytic Treatment of Pollutants in Aqueous Media. *Environ. Int.* **2016**, *91*, 94–103. https://doi.org/10.1016/j.envint.2016.02.012.

(6) Goodarzi, N.; Ashrafi-Peyman, Z.; Khani, E.; Moshfegh, A. Z. Recent Progress on Semiconductor Heterogeneous Photocatalysts in Clean Energy Production and Environmental Remediation. *Catalysts* **2023**, *13* (7), 1102. https://doi.org/10.3390/catal13071102.

(7) Sharma, P.; Hasan, M. R.; Mehto, N. K.; Deepak; Bishoyi, A.; Narang, J. 92 Years of Zinc Oxide: Has Been Studied by the Scientific Community since the 1930s- An Overview. *Sensors Int.* **2022**, *3*, 100182. https://doi.org/10.1016/j.sintl.2022.100182.

(8) Collard, X.; El Hajj, M.; Su, B.-L.; Aprile, C. Synthesis of Novel Mesoporous ZnO/SiO2 Composites for the Photodegradation of Organic Dyes. *Microporous Mesoporous Mater.* **2014**, *184*, 90–96. https://doi.org/10.1016/J.MICROMESO.2013.09.040.

(9) Puri, N.; Gupta, A. Water Remediation Using Titanium and Zinc Oxide Nanomaterials through Disinfection and Photo Catalysis Process: A Review. *Environ. Res.* **2023**, *227* (February), 115786. https://doi.org/10.1016/j.envres.2023.115786.

(10) Zheng, A. L. T.; Abdullah, C. A. C.; Chung, E. L. T.; Andou, Y. Recent Progress in Visible Light-Doped ZnO Photocatalyst for Pollution Control. *Int. J. Environ. Sci. Technol.* **2022**, *20* (5), 5753–5772. https://doi.org/10.1007/s13762-022-04354-x.

(11) Kheirabadi, M.; Samadi, M.; Asadian, E.; Zhou, Y.; Dong, C.; Zhang, J.; Moshfegh, A. Z. Well-Designed Ag/ZnO/3D Graphene Structure for Dye Removal: Adsorption, Photocatalysis and Physical Separation Capabilities. *J. Colloid Interface Sci.* **2019**, *537*, 66–78. https://doi.org/10.1016/J.JCIS.2018.10.102.

(12) Singh, J.; Soni, R. K. Controlled Synthesis of CuO Decorated Defect Enriched ZnO Nanoflakes for Improved Sunlight-Induced Photocatalytic Degradation of Organic Pollutants. *Appl. Surf. Sci.* **2020**, *521*, 146420. https://doi.org/10.1016/j.apsusc.2020.146420.

(13) Ab Wahab, N.; Sairi, N. A.; Alias, Y. Photocatalytic Activities Enhancement of Manganese Doped ZnO by Decoration on CNT for Degradation of Organic Pollutants under Solar Irradiation. *Appl. Phys. A* **2022**, *128* (1), 59. https://doi.org/10.1007/s00339-021-05160-x.

(14) Sin, J. C.; Lam, S. M.; Lee, K. T.; Mohamed, A. R. Fabrication of Erbium-Doped Spherical-like ZnO Hierarchical Nanostructures with Enhanced Visible Light-Driven Photocatalytic Activity. *Mater. Lett.* **2013**, *91*, 1–4. https://doi.org/10.1016/J.MATLET.2012.09.049.

(15) Wu, J.; Xue, D. Progress of Science and Technology of ZnO as Advanced Material. *Sci. Adv. Mater.* **2011**, *3* (2), 127–149. https://doi.org/10.1166/sam.2011.1144.

(16) Seid, E. T.; Dejene, F. B. Gallium and Indium Co-Doping Effects on Structural, Optical and Luminescence Properties of ZnO Nanostructures. *Mater. Today Commun.* **2021**, *27*,

102330. https://doi.org/10.1016/J.MTCOMM.2021.102330.

(17) Chen, L.; Yu, S.; Shen, G.; Tang, S.; Zhang, T.; Li, J. G.; Zhu, Q. Large-Scale Irrigation of Cr3+ into Different Octahedra of Zinc Aluminate toward Continual Broadband near-Infrared Emission. *Ceram. Int.* **2024**, *50* (1), 1956–1969. https://doi.org/10.1016/J.CERAMINT.2023.10.299.

(18) Huili, H.; Grindi, B.; Tahar, L. Ben. Influence of Fe Substitution by Al on the Structural, Microstructural, and Magnetic Properties of Co0.2Ni0.3Zn0.5Fe2O4 Nanoparticles. *J. Solid State Chem.* **2024**, *330*, 124495. https://doi.org/10.1016/j.jssc.2023.124495.

(19) Serier, H.; Demourgues, A.; Gaudon, M. Investigation of Ga Substitution in ZnO Powder and Opto-Electronic Properties. *Inorg. Chem.* **2010**, *49* (15), 6853–6858. https://doi.org/10.1021/ic1000733.

(20) Pham, A. T. T.; Trinh, L. T.; Pham, N. K.; Lai, H. T.; ... Effect of 0.5 At.% Indium on Thermoelectric Properties of Gallium Doped-Zinc Oxide Bulk. *Vietnam J. ...* **2020**, *58* (2), 175–180. https://doi.org/10.15625/2525-2518/58/2/14019.

(21) Ullah, M.; Bin Su, W.; Manan, A.; Ahmad, A. S.; Shah, A. A.; Yao, Z. Phase, Microstructural Investigation and Thermoelectric Properties of Ga-Doped Zinc Oxide-Based Ceramics Sintered under an Argon Atmosphere. *Ceram. Int.* **2018**, *44* (15), 17873–17877. https://doi.org/10.1016/J.CERAMINT.2018.06.259.

(22) Chongsri, K.; Pecharapa, W. Structural Properties of Ga-Doped ZnO Nanoparticles Synthesized by Co-Precipitation Process. *Integr. Ferroelectr.* **2015**, *165* (1), 159–166. https://doi.org/10.1080/10584587.2015.1063925.

(23) Wang, Y.; Zhang, M.; Ma, H.; Su, H.; Li, A.; Ruan, W.; Zhao, B. Surface Plasmon

Resonance from Gallium-Doped Zinc Oxide Nanoparticles and Their Electromagnetic Enhancement Contribution to Surface-Enhanced Raman Scattering. *ACS Appl. Mater. Interfaces* **2021**, *13* (29), 35038–35045. https://doi.org/10.1021/acsami.1c05804.

(24) Li, P.; Wang, X.; Zhang, X.; Zhang, L.; Yang, X.; Zhao, B. Investigation of the Charge-Transfer between Ga-Doped ZnO Nanoparticles and Molecules Using Surface-Enhanced Raman Scattering: Doping Induced Band-Gap Shrinkage. *Front. Chem.* **2019**, *7* (MAR), 144. https://doi.org/10.3389/FCHEM.2019.00144/BIBTEX.

(25) Pham, A. T. T.; Luu, T. A.; Pham, N. K.; Ta, H. K. T.; Nguyen, T. H.; Van Hoang, D.; Lai, H. T.; Tran, V. C.; Park, J. H.; Lee, J. K.; Park, S.; Michitaka, O.; Park, S. D.; Nguyen, H. Q.; Phan, T. B. Multi-Scale Defects in ZnO Thermoelectric Ceramic Materials Co-Doped with In and Ga. *Ceram. Int.* **2020**, *46* (8), 10748–10758. https://doi.org/10.1016/j.ceramint.2020.01.084.

(26) Shinde, S. S.; Shinde, P. S.; Oh, Y. W.; Haranath, D.; Bhosale, C. H.; Rajpure, K. Y. Structural, Optoelectronic, Luminescence and Thermal Properties of Ga-Doped Zinc Oxide Thin Films. *Appl. Surf. Sci.* **2012**, *258* (24), 9969–9976. https://doi.org/10.1016/j.apsusc.2012.06.058.

(27) Al Ghafry, S. S. A.; Al-Abri, M. Z.; Al Farsi, B.; Al Marzouqi, F.; Al Farsi, L. M.; Roslan, N. A.; Supangat, A. Ga-Doped ZnO Nanorods: The Photocatalytic Performance of Methylene Blue under Solar Irradiation. *Opt. Mater. (Amst).* **2022**, *126* (February), 112139. https://doi.org/10.1016/j.optmat.2022.112139.

(28) Cardoza-Contreras, M. N.; Vásquez-Gallegos, A.; Vidal-Limon, A.; Romo-Herrera, J. M.; Águila, S.; Contreras, O. E. Photocatalytic and Antimicrobial Properties of Ga Doped and Ag Doped ZnO Nanorods for Water Treatment. *Catalysts* **2019**, *9* (2).

https://doi.org/10.3390/catal9020165.

(29) Farha, A. H.; Ibrahim, M. M.; Mansour, S. A. Ga-Doped ZnO Nanostructured Powder for Cool-Nanopigment in Environment Applications. *Materials (Basel)*. **2020**, *13* (22), 5152. https://doi.org/10.3390/ma13225152.

(30) D, N.; Kondamareddy, K. K.; Bin, H.; Lu, D.; Kumar, P.; Dwivedi, R. K.; Pelenovich, V. O.; Zhao, X.-Z.; Gao, W.; Fu, D. Enhanced Visible Light Photodegradation Activity of RhB/MB from Aqueous Solution Using Nanosized Novel Fe-Cd Co-Modified ZnO. *Sci. Rep.* **2018**, *8* (1), 10691. https://doi.org/10.1038/s41598-018-29025-1.

(31) Wang, J.; Han, A.; Jaenicke, S.; Chuah, G. K. *Advances in Sorbents and Photocatalytic Materials for Water Remediation*; Elsevier B.V., 2013. https://doi.org/10.1016/B978-0-444-53870-3.00006-X.

(32) Lai, Y.; Meng, M.; Yu, Y.; Wang, X.; Ding, T. Photoluminescence and Photocatalysis of the Flower-like Nano-ZnO Photocatalysts Prepared by a Facile Hydrothermal Method with or without Ultrasonic Assistance. *Appl. Catal. B Environ.* **2011**, *105* (3–4), 335–345. https://doi.org/10.1016/j.apcatb.2011.04.028.

(33) Chiu, H.-M.; Yang, T.-H.; Hsueh, Y.-C.; Perng, T.-P.; Wu, J.-M. Fabrication and Characterization of Well-Dispersed Plasmonic Pt Nanoparticles on Ga-Doped ZnO Nanopagodas Array with Enhanced Photocatalytic Activity. *Appl. Catal. B Environ.* **2015**, *163*, 156–166. https://doi.org/10.1016/j.apcatb.2014.07.039.

(34) Chiang, J.-L.; Yadlapalli, B. K.; Chen, M.-I.; Wuu, D.-S. A Review on Gallium Oxide Materials from Solution Processes. *Nanomaterials* **2022**, *12* (20), 3601. https://doi.org/10.3390/nano12203601.

(35) Luchechko, A.; Vasyltsiv, V.; Kushlyk, M.; Slobodzyan, D.; Baláž, M.; Cebulski, J.; Szmuc, K.; Szlęzak, J.; Shpotyuk, Y. Structural and Luminescence Characterization of β-Ga2O3 Nanopowders Obtained via High-Energy Ball Milling. *Appl. Nanosci.* **2022**, No. 0123456789. https://doi.org/10.1007/s13204-022-02717-x.

(36) Roy, R.; Hill, V. G.; Osborn, E. F. Polymorphism of Ga2O3and the System Ga2O3−H2O. *J. Am. Chem. Soc.* **1952**, *74* (3), 719–722. https://doi.org/10.1021/ja01123a039.

(37) Xu, J.; Zheng, W.; Huang, F. Gallium Oxide Solar-Blind Ultraviolet Photodetectors: A Review. *J. Mater. Chem. C* **2019**, *7* (29), 8753–8770. https://doi.org/10.1039/C9TC02055A.

(38) Huang, Z.; Zhou, S.; Chen, L.; Zheng, Q.; Li, H.; Xiong, Y.; Ye, L.; Kong, C.; Fan, S.; Zhang, H.; Li, W. Fully Transparent Amorphous Ga2O3-Based Solar-Blind Ultraviolet Photodetector with Graphitic Carbon Electrodes. *Crystals* **2022**, *12* (10), 1427. https://doi.org/10.3390/cryst12101427.

(39) Jamarkattel, M. K.; Phillips, A. B.; Subedi, I.; Abudulimu, A.; Bastola, E.; Li, D.-B.; Mathew, X.; Yan, Y.; Ellingson, R. J.; Podraza, N. J.; Heben, M. J. Indium Gallium Oxide Emitters for High-Efficiency CdTe-Based Solar Cells. *ACS Appl. Energy Mater.* **2022**, *5* (5), 5484–5489. https://doi.org/10.1021/acsaem.2c00153.

(40) Chua, D.; Kim, S. B.; Gordon, R. Enhancement of the Open Circuit Voltage of Cu 2 O/Ga 2 O 3 Heterojunction Solar Cells through the Mitigation of Interfacial Recombination. *AIP Adv.* **2019**, *9* (5), 055203. https://doi.org/10.1063/1.5096283.

(41) Adams, W. T.; Ivanisevic, A. Nanostructured Oxides Containing Ga: Materials with Unique Properties for Aqueous-Based Applications. *ACS Omega* **2019**, *4* (4), 6876–

6882. https://doi.org/10.1021/acsomega.9b00461.

(42) Ghodsi, V.; Jin, S.; Byers, J. C.; Pan, Y.; Radovanovic, P. V. Anomalous Photocatalytic Activity of Nanocrystalline γ-Phase Ga2O3 Enabled by Long-Lived Defect Trap States. *J. Phys. Chem. C* **2017**, *121* (17), 9433–9441. https://doi.org/10.1021/acs.jpcc.7b02275.

(43) Ratcliff, L. E.; Oshima, T.; Nippert, F.; Janzen, B. M.; Kluth, E.; Goldhahn, R.; Feneberg, M.; Mazzolini, P.; Bierwagen, O.; Wouters, C.; Nofal, M.; Albrecht, M.; Swallow, J. E. N.; Jones, L. A. H.; Thakur, P. K.; Lee, T.-L.; Kalha, C.; Schlueter, C.; Veal, T. D.; Varley, J. B.; Wagner, M. R.; Regoutz, A. Tackling Disorder in Gamma-Ga2O3. **2022**.

(44) Playford, H. Y.; Hannon, A. C.; Tucker, M. G.; Dawson, D. M.; Ashbrook, S. E.; Kastiban, R. J.; Sloan, J.; Walton, R. I. Characterization of Structural Disorder in γ-Ga2O3. *J. Phys. Chem. C* **2014**, *118* (29), 16188–16198. https://doi.org/10.1021/jp5033806.

(45) Martínez-Criado, G.; Segura-Ruiz, J.; Chu, M.-H.; Tucoulou, R.; López, I.; Nogales, E.; Mendez, B.; Piqueras, J. Crossed Ga 2 O 3 /SnO 2 Multiwire Architecture: A Local Structure Study with Nanometer Resolution. *Nano Lett.* **2014**, *14* (10), 5479–5487. https://doi.org/10.1021/nl502156h.

(46) Morkoç, H.; Özgür, Ü. *Zinc Oxide*; Wiley, 2009; Vol. 13. https://doi.org/10.1002/9783527623945.

(47) Gupta, H.; Singh, J.; Dutt, R. N.; Ojha, S.; Kar, S.; Kumar, R.; Reddy, V. R.; Singh, F. Defect-Induced Photoluminescence from Gallium-Doped Zinc Oxide Thin Films: Influence of Doping and Energetic Ion Irradiation. *Phys. Chem. Chem. Phys.* **2019**, *21* (27), 15019–15029. https://doi.org/10.1039/C9CP02148E.

(48) Li, X.; Hu, Z.; Liu, J.; Li, D.; Zhang, X.; Chen, J.; Fang, J. Ga Doped ZnO Photonic Crystals with Enhanced Photocatalytic Activity and Its Reaction Mechanism. *Appl. Catal. B Environ.* **2016**, *195*, 29–38. https://doi.org/10.1016/j.apcatb.2016.05.002.

(49) Gaffuri, P.; Dedova, T.; Appert, E.; Danilson, M.; Baillard, A.; Chaix-Pluchery, O.; Güell, F.; Oja-Acik, I.; Consonni, V. Enhanced Photocatalytic Activity of Chemically Deposited ZnO Nanowires Using Doping and Annealing Strategies for Water Remediation. *Appl. Surf. Sci.* **2022**, *582*, 152323. https://doi.org/10.1016/j.apsusc.2021.152323.

(50) Piras, A.; Olla, C.; Reekmans, G.; Kelchtermans, A.-S.; De Sloovere, D.; Elen, K.; Carbonaro, C. M.; Fusaro, L.; Adriaensens, P.; Hardy, A.; Aprile, C.; Van Bael, M. K. Photocatalytic Performance of Undoped and Al-Doped ZnO Nanoparticles in the Degradation of Rhodamine B under UV-Visible Light:The Role of Defects and Morphology. *Int. J. Mol. Sci.* **2022**, *23* (24), 15459. https://doi.org/10.3390/ijms232415459.

(51) Marchelek, M.; Diak, M.; Kozak, M.; Zaleska-Medynska, A.; Grabowska, E. Some Unitary, Binary, and Ternary Non-TiO2 Photocatalysts. In *Semiconductor Photocatalysis - Materials, Mechanisms and Applications*; InTech, 2016. https://doi.org/10.5772/62583.

(52) Thomas, G. S.; Kamath, P. V. The Layered Double Hydroxide (LDH) of Zn with Ga: Synthesis and Reversible Thermal Behaviour. *Solid State Sci.* **2006**, *8* (10), 1181–1186. https://doi.org/10.1016/j.solidstatesciences.2006.03.006.

(53) Hammann, B. A.; Ma, Z. L.; Wentz, K. M.; Kamunde-Devonish, M. K.; Johnson, D. W.; Hayes, S. E. Structural Study by Solid-State ^{71} Ga NMR of Thin Film Transistor

Precursors. *Dalt. Trans.* **2015**, *44* (40), 17652–17659. https://doi.org/10.1039/C5DT02967H.

(54) Mackenzie, K. J. D.; Smith, M. E. *Multinuclear Solid-State NMR of Inorganic Materials*, PERGAMON M.; Cahn, R. W., Ed.; Pergamon, 2002.

(55) Areán, C. O.; Delgado, M. R.; Montouillout, V.; Massiot, D. Synthesis and Characterization of Spinel-Type Gallia-Alumina Solid Solutions. *Zeitschrift für Anorg. und Allg. Chemie* **2005**, *631* (11), 2121–2126. https://doi.org/10.1002/zaac.200570027.

(56) Docherty, S. R.; Völker, L. A.; Yakimov, A. V.; Verel, R.; Copéret, C. 71 Ga NMR Signatures of Lewis and Brønsted Acid Sites in Gallium Silicates Evidenced and Deciphered upon Interaction with Probe Molecules. *J. Phys. Chem. C* **2023**, *127* (51), 24552–24563. https://doi.org/10.1021/acs.jpcc.3c05638.

(57) Ponja, S. D.; Sathasivam, S.; Parkin, I. P.; Carmalt, C. J. Highly Conductive and Transparent Gallium Doped Zinc Oxide Thin Films via Chemical Vapor Deposition. *Sci. Rep.* **2020**, *10* (1), 638. https://doi.org/10.1038/s41598-020-57532-7.

(58) Wu, H. C.; Peng, Y. C.; Chen, C. C. Effects of Ga Concentration on Electronic and Optical Properties of Ga-Doped ZnO from First Principles Calculations. *Opt. Mater. (Amst).* **2013**, *35* (3), 509–515. https://doi.org/10.1016/J.OPTMAT.2012.10.022.

(59) Bernardo, M. S.; Villanueva, P. G.; Jardiel, T.; Calatayud, D. G.; Peiteado, M.; Caballero, A. C. Ga-Doped ZnO Self-Assembled Nanostructures Obtained by Microwave-Assisted Hydrothermal Synthesis: Effect on Morphology and Optical Properties. *J. Alloys Compd.* **2017**, *722*, 920–927. https://doi.org/10.1016/j.jallcom.2017.06.160.

(60) Pradhan, N.; Das Adhikari, S.; Nag, A.; Sarma, D. D. Luminescence, Plasmonic, and Magnetic Properties of Doped Semiconductor Nanocrystals. *Angew. Chem. Int. Ed. Engl.* **2017**, *56* (25), 7038–7054. https://doi.org/10.1002/anie.201611526.

(61) Ben Moussa, N.; Lajnef, M.; Jebari, N.; Villebasse, C.; Bayle, F.; Chaste, J.; Madouri, A.; Chtourou, R.; Herth, E. Synthesis of ZnO Sol–Gel Thin-Films CMOS-Compatible. *RSC Adv.* **2021**, *11* (37), 22723–22733. https://doi.org/10.1039/D1RA02241E.

(62) Calzolari, A.; Nardelli, M. B. Dielectric Properties and Raman Spectra of ZnO from a First Principles Finite-Differences/Finite-Fields Approach. *Sci. Rep.* **2013**, *3* (1), 2999. https://doi.org/10.1038/srep02999.

(63) Janzen, B. M.; Mazzolini, P.; Gillen, R.; Peltason, V. F. S.; Grote, L. P.; Maultzsch, J.; Fornari, R.; Bierwagen, O.; Wagner, M. R. Comprehensive Raman Study of Orthorhombic κ/ε-Ga2O3and the Impact of Rotational Domains. *J. Mater. Chem. C* **2021**, *9* (40), 14175–14189. https://doi.org/10.1039/d1tc03500b.

(64) Kim, J.; Dutta, A.; Memarzadeh, B.; Kildishev, A. V.; Mosallaei, H.; Boltasseva, A. Zinc Oxide Based Plasmonic Multilayer Resonator: Localized and Gap Surface Plasmon in the Infrared. *ACS Photonics* **2015**, *2* (8), 1224–1230. https://doi.org/10.1021/acsphotonics.5b00318.

(65) Della Gaspera, E.; Chesman, A. S. R.; van Embden, J.; Jasieniak, J. J. Non-Injection Synthesis of Doped Zinc Oxide Plasmonic Nanocrystals. *ACS Nano* **2014**, *8* (9), 9154–9163. https://doi.org/10.1021/nn5027593.

(66) Ristić, M.; Popović, S.; Musić, S. Application of Sol-Gel Method in the Synthesis of Gallium(III)-Oxide. *Mater. Lett.* **2005**, *59* (10), 1227–1233. https://doi.org/10.1016/j.matlet.2004.11.055.

(67) Gopal, R.; Goyal, A.; Saini, A.; Nagar, M.; Sharma, N.; Gupta, D. K.; Dhayal, V. Sol-Gel Synthesis of Ga2O3 Nanorods and Effect of Precursor Chemistry on Their Structural and Morphological Properties. *Ceram. Int.* **2018**, *44* (16), 19099–19105. https://doi.org/10.1016/j.ceramint.2018.07.173.

(68) Shi, F.; Qiao, H. Influence of Hydrothermal Reaction Time on Crystal Qualities and Photoluminescence Properties of β-Ga2O3 Nanorods. *J. Mater. Sci. Mater. Electron.* **2020**, *31* (22), 20223–20231. https://doi.org/10.1007/s10854-020-04542-w.

(69) Onuma, T.; Saito, S.; Sasaki, K.; Goto, K.; Masui, T.; Yamaguchi, T.; Honda, T.; Kuramata, A.; Higashiwaki, M. Temperature-Dependent Exciton Resonance Energies and Their Correlation with IR-Active Optical Phonon Modes in β-Ga2O3 Single Crystals. *Appl. Phys. Lett.* **2016**, *108* (10). https://doi.org/10.1063/1.4943175.

(70) Usseinov, A.; Koishybayeva, Z.; Platonenko, A.; Pankratov, V.; Suchikova, Y.; Akilbekov, A.; Zdorovets, M.; Purans, J.; Popov, A. I. Vacancy Defects in Ga2O3: First-Principles Calculations of Electronic Structure. *Materials (Basel).* **2021**, *14* (23). https://doi.org/10.3390/ma14237384.

(71) Janzen, B. M.; Mazzolini, P.; Gillen, R.; Falkenstein, A.; Martin, M.; Tornatzky, H.; Maultzsch, J.; Bierwagen, O.; Wagner, M. R. Isotopic Study of Raman Active Phonon Modes in β-Ga 2 O 3. *J. Mater. Chem. C* **2021**, *9* (7), 2311–2320. https://doi.org/10.1039/D0TC04101G.

(72) Rodrigues, A. V.; Sabino, N. L. Synthesis of Photoluminescent β-Ga2O3 Nanostructures Using Electrospinning Method, and Control of Length-Diameter Ratio by Calcination Heating Rates. *J. Mater. Sci. Mater. Electron.* **2019**, *30* (18), 16910–16916. https://doi.org/10.1007/s10854-019-01631-3.

(73) Al-Buriahi, A. K.; Al-Gheethi, A. A.; Senthil Kumar, P.; Radin Mohamed, R. M. S.; Yusof, H.; Alshalif, A. F.; Khalifa, N. A. Elimination of Rhodamine B from Textile Wastewater Using Nanoparticle Photocatalysts: A Review for Sustainable Approaches. *Chemosphere* **2022**, *287*, 132162. https://doi.org/10.1016/j.chemosphere.2021.132162.

(74) Benamara, M.; Nassar, K. I.; Essid, M.; Frick, S.; Rugmini, R.; Sekhar, K. C.; Silva, J. P. B. B. Visible Light-Driven Removal of Rhodamine B Using Indium-Doped Zinc Oxide Prepared by Sol–Gel Method. *J. Sol-Gel Sci. Technol.* **2024**, *111* (2), 553–565. https://doi.org/10.1007/s10971-024-06471-0.

(75) Haleem, A.; Ullah, M.; Rehman, S. ur; Shah, A.; Farooq, M.; Saeed, T.; Ullah, I.; Li, H. In-Depth Photocatalytic Degradation Mechanism of the Extensively Used Dyes Malachite Green, Methylene Blue, Congo Red, and Rhodamine B via Covalent Organic Framework-Based Photocatalysts. *Water* **2024**, *16* (11), 1588. https://doi.org/10.3390/w16111588.

(76) Yu, K.; Yang, S.; He, H.; Sun, C.; Gu, C.; Ju, Y. Visible Light-Driven Photocatalytic Degradation of Rhodamine B over NaBiO 3 : Pathways and Mechanism. *J. Phys. Chem. A* **2009**, *113* (37), 10024–10032. https://doi.org/10.1021/jp905173e.

(77) Dodoo-Arhin, D.; Asiedu, T.; Agyei-Tuffour, B.; Nyankson, E.; Obada, D.; Mwabora, J. M. Photocatalytic Degradation of Rhodamine Dyes Using Zinc Oxide Nanoparticles. *Mater. Today Proc.* **2021**, *38*, 809–815. https://doi.org/10.1016/j.matpr.2020.04.597.

(78) Zanatta, A. R. Revisiting the Optical Bandgap of Semiconductors and the Proposal of a Unified Methodology to Its Determination. *Sci. Rep.* **2019**, *9* (1), 11225. https://doi.org/10.1038/s41598-019-47670-y.

(79) Shi, F.; Qiao, H. Preparations, Properties and Applications of Gallium Oxide

Nanomaterials – A Review. *Nano Sel.* **2022**, *3* (2), 348–373. https://doi.org/10.1002/nano.202100149.

(80) Viandĺlora, E. G.; Yamaga, M.; Inoue, T.; Yabasi, S.; Masui, Y.; Sugawara, T.; Fukuda, T. Optical Spectroscopy Study on β-Ga2O3. *Japanese J. Appl. Physics, Part 2 Lett.* **2002**, *41* (6 A), 622–625. https://doi.org/10.1143/jjap.41.l622.

(81) Tong, J.; Risbud, S. H. Processing and Structure of Gallium Nitride—Gallium Oxide Platelet Nanostructures. *J. Solid State Chem.* **2004**, *177* (10), 3568–3574. https://doi.org/10.1016/J.JSSC.2004.06.025.

(82) Wang, T.; Radovanovic, P. V. Size-Dependent Electron Transfer and Trapping in Strongly Luminescent Colloidal Gallium Oxide Nanocrystals. *J. Phys. Chem. C* **2011**, *115* (38), 18473–18478. https://doi.org/10.1021/jp205502d.

(83) Chen, T.; Tang, K. γ- Ga2O3 Quantum Dots with Visible Blue-Green Light Emission Property. *Appl. Phys. Lett.* **2007**, *90* (5), 2–5. https://doi.org/10.1063/1.2437110.

(84) Le Thi Thanh, T.; Nguyen Thi, L.; Tran Dinh, T.; Nguyen Van, N. Enhanced Photocatalytic Degradation of Rhodamine B Using C/Fe Co-Doped Titanium Dioxide Coated on Activated Carbon. *J. Chem.* **2019**, *2019*, 1–8. https://doi.org/10.1155/2019/2949316.

(85) Skillen, N.; Rice, C.; Pang, X.; Robertson, P. K. J.; McCormick, W.; McCrudden, D. *Photocatalytic Radical Species: An Overview of How They Are Generated, Detected, and Measured*; Elsevier B.V., 2021. https://doi.org/10.1016/B978-0-12-823007-7.00008-0.

SYNOPSIS

This study systematically explores Ga-doped ZnO nanomaterials, focusing on their structure-response under UV-green light irradiation. The findings reveal that gallium doping results in favorable photoluminescence and photocatalytic properties with minimal oxygen vacancy variation. Analyzing gallium incorporation and coordination variations highlights the importance of defect engineering. Using Rhodamine B photodegradation as a test reaction, the study shows the comparable catalytic activity of Ga-doped and undoped ZnO, advancing knowledge in (photo-)catalytic design and applications.

GRAPHICAL ABSTRACT

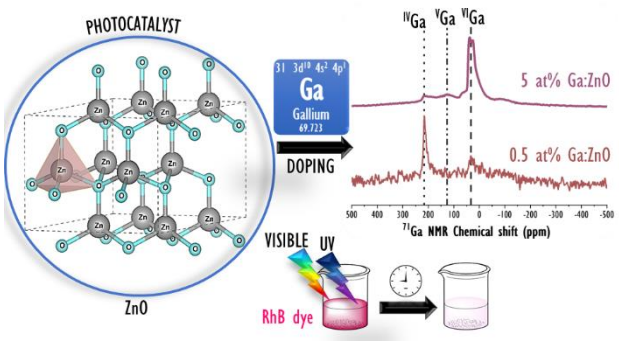

For table of contents only